

PRIMARY TRANSIT OF THE PLANET HD189733B AT 3.6 AND 5.8 μ MJ.P. BEAULIEU^{1,2}, S. CAREY³, I. RIBAS^{4,2}, G. TINETTI^{5,2}

ABSTRACT

The hot Jupiter HD 189733b was observed during its primary transit using the Infrared Array Camera on the *Spitzer Space Telescope*. The transit depths were measured simultaneously at 3.6 and 5.8 μ m. Our analysis yields values of $2.356 \pm 0.019\%$ and $2.436 \pm 0.020\%$ at 3.6 and 5.8 μ m respectively, for a uniform source. We estimated the contribution of the limb-darkening and star-spot effects on the final results. We concluded that although the limb darkening increases by ~ 0.02 - 0.03% the transit depths, and the differential effects between the two IRAC bands is even smaller, 0.01% . Furthermore, the host star is known to be an active spotted K star with observed photometric modulation. If we adopt an extreme model of 20% coverage with spots 1000K cooler of the star surface, it will make the observed transits shallower by 0.19 and 0.18% . The difference between the two bands will be only of 0.01% , in the opposite direction to the limb darkening correction. If the transit depth is affected by limb darkening and spots, the differential effects between the 3.6 and 5.8 μ m bands are very small. The differential transit depths at 3.6 and 5.8 μ m and the recent one published by Knutson et al. (2007) at 8 μ m are in agreement with the presence of water vapour in the upper atmosphere of the planet. This is the companion paper to Tinetti et al. (2007b), where the detailed atmosphere models are presented.

Subject headings: Stars: planetary systems — planetary systems: formation — *Facilities:* Spitzer

1. INTRODUCTION

Over 240 planets are now known to orbit stars different from our Sun (Schneider 2007; Butler et al. 2007). This number is due to increase exponentially in the near future thanks to space-missions devoted to the detection of exoplanets and the improved capabilities of the ground-based telescopes. Among the exoplanets discovered so far, the best known class of planetary bodies are giant planets (EGPs) orbiting very close-in (hot-Jupiters). In particular, hot-Jupiters that transit their parent stars offer a unique opportunity to estimate directly key physical properties of their atmospheres (Brown, 2001). In particular, the use of the primary transit (when the planet passes in front of its parent star) and transmission spectroscopy to probe the upper layers of the transiting EGPs, has been particularly successful in the UV and visible ranges (Charbonneau et al. 2002; Richardson et al. 2003, 2003a; Deming et al. 2005a; Vidal-Madjar et al. 2003, 2004; Knutson et al. 2007; Ballester, Sing, & Herbert 2007; Ben-Jaffel, 2007) and in the thermal IR (Richardson et al. 2006; Knutson et al. 2007).

The hot-Jupiter HD 189733b (Bouchy et al. 2005) has a mass of $M_p = 1.15 \pm 0.04 M_{\text{Jup}}$, a radius of $R_p = 1.26 \pm 0.03 R_{\text{Jup}}$, and orbits a main sequence K-type star at a distance of 0.0312 AU . This exoplanet is orbiting the brightest and closest star discovered so far, making it one of the prime targets for observations (Bakos et al. 2006; Winn et al. 2007; Deming et al. 2006; Grillmair et al. 2007; Knutson et al. 2007).

Tinetti et al. (2007a) have modeled the infrared transmission spectrum of the planet HD 189733b during the primary transit and have shown that *Spitzer* observations are well suited to probe the atmospheric composition and, in particular, constrain the abundances of water vapor and CO. Here we analyze the observations of HD 189733b with the Infrared Array Camera (IRAC Fazio et al., 2004) on board the *Spitzer* Space Telescope in two bands centered at 3.6 and 5.8 μ m. We report the data reduction, and discuss our results in light of the theoretical predictions and the recent observation at 8 μ m (Knutson et al. 2007).

2. METHODS

2.1. The observations

HD 189733 was observed on October 31, 2006 (program id 30590) during the primary transit of its planet with the IRAC instrument. During the 4.5 hours of observations, 1.8 hours were spent on the planetary transit, and 2.7 hours outside the transit. High accuracy in the relative photometry was obtained so that the transit data in the two bands could be compared. During the observations, the pointing was held constant to keep the source centered on a given pixel of the detector. Two reasons prompted us to adopt this approach:

- The amount of light detected in channel 1 shows variability that depends on the relative position of the source with respect to a pixel center (called the pixel-phase effect). This effect could be up to 4% peak-to-peak at 3.6 μ m. Corrective terms have been determined for channel 1 and are reported in the IRAC Manual, but also by Morales-Calderón et al. (2006; hereafter MC06). These systematic effects are known to be variable across the field. At first order we can correct them using the prescriptions of MC06 or of the manual, and then check for the need of higher order corrections.

¹ Institut d'astrophysique de Paris, CNRS (UMR 7095), Université Pierre & Marie Curie, Paris, France

² HOLMES collaboration

³ IPAC-Spitzer Science Center, California Institute of Technology, Pasadena, California 91125, USA

⁴ Institut de Ciències de l'Espai (CSIC-IEEC), Campus UAB, 08193 Bellaterra, Spain

⁵ European Space Agency/University College London, Gower Street, London WC1E 6BT, UK

- Flat-fielding errors are another important issue. Observations at different positions on the array will cause a systematic scatter in the photometric data which may swamp the weak signal we are aiming to detect.

Therefore, to achieve high-precision photometry at $3.6\ \mu\text{m}$, it is important to keep the source fixed at a particular position in the array. Staring mode observations can keep a source fixed within 0.15 arcsecond. It is crucial to have pre-transit and post-transit data to estimate the systematic effects and to understand how to correct for them.

There is no significant pixel-phase effect for channel 3 of IRAC. However, the constraint on the flat-fielding error requires that the source is centered on the same pixel of the detector during the observations. A latent buildup may affect the response of the detector as a function of time. To avoid the saturation of the detector for this $K = 5.5$ mag target, a short exposure time was used. The observations were split in consecutive sub-exposures each integrated over 0.4 and 2 seconds for channel 1 and 3, respectively.

2.2. Data reduction

We used the flat-fielded, cosmic ray-corrected and flux-calibrated data files provided by the *Spitzer* pipeline. We treated the data of the two channels separately. We used the BLUE software (Alard 2007) which performs PSF photometry. Below we describe the details of this approach.

The PSF was reconstructed from a compilation of the brightest, unsaturated stars in the image. Once the local background had been subtracted and the flux normalized, we obtained a data set representing the PSF at different locations on the image. An analytical model was fitted to this dataset by using an expansion of Gaussian polynomial functions. To fit the PSF spatial variations, the coefficients of the local expansion are polynomial functions of the position in the image. Note that the functions used for the expansion of the PSF are similar to those used for the kernel expansion in the image subtraction process. A full description of this analytical scheme is given in Alard (2000).

The position of the centroid was quantified by an iterative process. Starting from an estimate, based on the position of the local maximum of the object, we performed a linear fit of the amplitude and the PSF offsets (dx, dy) to correct the position. The basic functions for this fit were the PSF and its first two derivatives. Note that in general the calculation of the PSF derivatives from its analytical model is numerically sensitive. We recall also that the first moments are exactly the PSF derivatives in the case of a Gaussian PSF. This procedure converges quickly: only few iterations are necessary for an accuracy of less than 1/100 of a pixel.

We performed photometry on all the frames of ch1 and ch3. We tried two different approaches: we used a Poisson weighting of the PSF fits and then the weight maps provided by the *Spitzer* pipeline. These maps contain for each pixel the propagated errors of the different steps through the *Spitzer* pipeline. The results of these two processing runs are almost indistinguishable. Systematic trends were present in both channels. Here we discuss

each channel separately.

3. RESULTS

3.1. Channel 1

Figure 1 shows the different steps of the data processing. In the upper panel we report the raw photometry as produced by BLUE. Inspection of the lightcurve in the pre-transit and post-transit phases shows systematic trends with time scales of about 1 hour, with a peak-to-peak amplitude of 0.7%, related to the variation of the pixel-phase due to the jitter of the satellite. The middle panel shows the pixel-phase. We can clearly see that the flux in the upper panel is correlated with the pixel-phase. We adopted the MC06 prescription to correct for the pixel-phase, and show the results binned by 10. Most of the systematic trends present in the raw photometry are removed, but not entirely. There are still some trends present for the lowest value of the pixel phase during the transit, pre-transit, and post-transit. Therefore, we used the pre and post-transit data to fit the corrective terms, as in the approach of MC06, and applied them to the full light curve. The results are shown in the lower panel of Fig. 1. There is an improvement in the baseline, and also in the transit. The central part of the transit has still four consecutive points deviating by $1-2\ \sigma$ around $t \sim 200$ s, corresponding to the lowest phase value. They are shown on Fig. 1 but we will exclude them from further analysis (Fig. 3). These remaining systematic effects are due to the phase. We ran calculations both by including these points and by excluding them, and then compared the results. Also, we adopted different binning: by 5, 10, 20 or 50 points. The results are compatible within the errorbars. As we discuss in more detail below, limb darkening effects are very small at $3.6\ \mu\text{m}$ so the shape of the transit light-curve is box-like.

3.2. Channel 3

In Fig. 2 we report the raw (upper panel) and the final (lower panel) photometric data. There is no correlation with the pixel-phase, but a long term systematic trend can be seen both out of and in the transit. This trend does not appear to be caused by a latent buildup, but it is probably linked to the variation of response of the pixels due to a long period of illumination. We used the pre-transit and the post-transit data to fit a linear corrective term that we applied to all the data. The results, binned by 10, are shown in the lower panel of Fig.2.

4. DISCUSSION

4.1. Comments about the data reduction

Using the BLUE software we carried out a full modeling of the PSF and obtained an optimal centroid determination. With an undersampled PSF, in data sets with strong pixel-phase effects (channels 1 and 2 from *Spitzer*), accurate centroid determination is a key issue for achieving high precision photometry.

In order to tackle the systematic trends that are present in IRAC observations, it is important to have sufficient baseline observations to analyze transit data. Here, it has been vital to have sufficient pre-transit and post-transit data in order to be able to check the nature of the systematics and correct for them. The 4.5 hours of observations were centered on 1.8 hours transit. Given

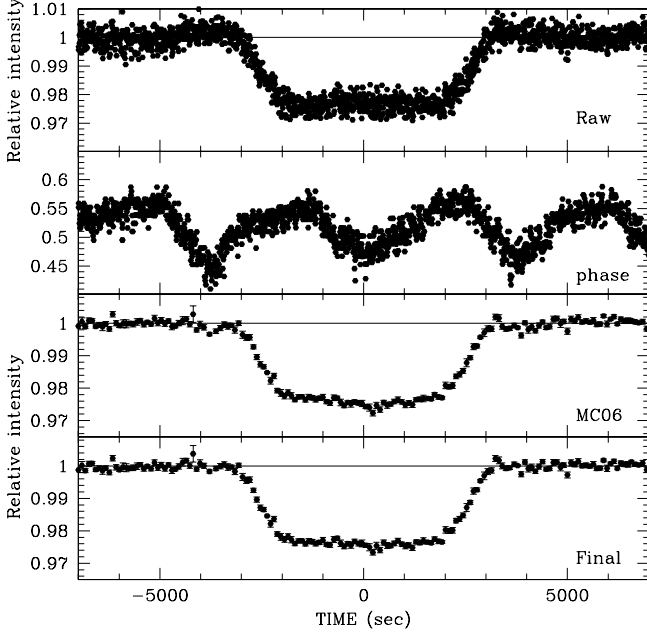


FIG. 1.— Top panel: raw photometric light curve, with systematic trends due to the pixel-phase effect. Middle panel: variation of the pixel-phase as a function of time. We can clearly see some correlations between these two panels, as expected from the known behavior of the IRAC Channel 1. Bottom panels: data binned by 10 after the correction for the pixel-phase. In the MC06 labeled panel we corrected the raw photometry using the prescription of Morales-Calderón et al. (2006). In the lowest panel, we estimated the corrective terms from pre-transit and post-transit data, and applied them to the full data set.

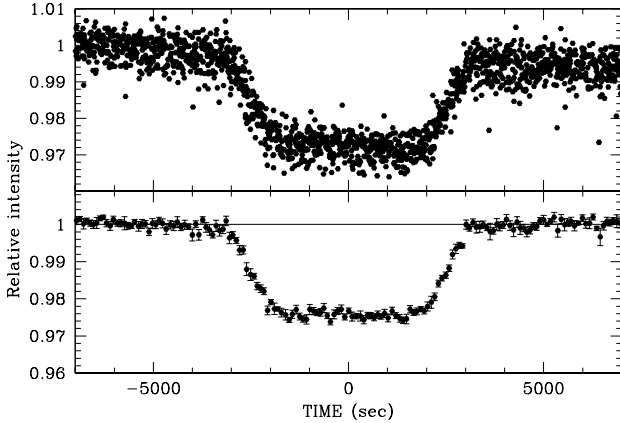


FIG. 2.— Upper panel: raw photometric light curve with a long term systematic trend. Lower panel: we estimated the corrective terms from pre-transit and post-transit data, and applied them to the full data set. We then bin the data by 10, and estimated the associated errorbar for each measurement.

the ~ 1 hour time scale of the pixel-phase variations, this was well adapted, but it is clearly a lower limit on the necessary observing time scale to achieve such observations.

4.2. Calculation of the transit depth

We decide to do a direct comparison between the out-of-transit flux (Fig. 1 and Fig. 2) and the in-transit flux (the central 3500 sec) averaged over its flat part for each channel. We estimate the weighted mean and its error

TABLE 1
LIMB DARKENING COEFFICIENTS

| IRAC | C1 | C2 | C3 | C4 |
|-------------------|--------|---------|--------|---------|
| 3.6 μm | 0.6023 | -0.5110 | 0.4655 | -0.1752 |
| 5.8 μm | 0.7137 | -1.0720 | 1.0515 | -0.3825 |

TABLE 2
FITTING PARAMETERS OF THE TRANSIT CURVES

| Parameter | 3.6 μm | 5.8 μm |
|-------------------------------|----------------------|---------------------|
| R_p/R_\star (LD) | 0.15285 ± 0.0003 | 0.1545 ± 0.0004 |
| b | 0.620 ± 0.01 | 0.620 ± 0.01 |
| $(R_p/R_\star)^2$ % (Uniform) | 2.356 ± 0.019 | 2.436 ± 0.023 |
| $(R_p/R_\star)^2$ % (LD) | 2.383 ± 0.014 | 2.457 ± 0.017 |

both in the out-of-transit flux and the in-transit flux. For channel 1, we have excluded the measurements obtained at the lowest pixel phase values as discussed in 3.1. It yields values of $2.356 \pm 0.019\%$ and $2.436 \pm 0.020\%$ in the 3.6- and 5.8- μm bands, respectively (fig. 4). This is the same approach as adopted by Knutson et al. (2007).

4.3. Contribution of limb-darkening

As a further refinement in our analysis we considered the effects of limb darkening. By inspection, the transit is clearly flat bottomed, and limb darkening was expected to be negligible. However, it was deemed worth calculating its contribution because of the high accuracy claimed in the transit depth measurement given above. We adopted a non-linear limb darkening law model as described in Mandel & Agol (2002) to calculate a limb-darkened light curve. We considered the more sophisticated form using four coefficients (C_1 , C_2 , C_3 , and C_4). These were calculated using a Kurucz (2005) stellar model ($T_{\text{eff}} = 5000$ K, $\log g = 4.5$, solar abundance), which matches closely the observed parameters of HD 189733, convolved with the IRAC passbands. Parameters are given in Table 1.

A multi-parameter fit of the two light curves using the adopted non-linear limb-darkening model yielded depths of $2.387 \pm 0.014\%$ and $2.456 \pm 0.017\%$ in the 3.6- and 5.8- μm bands, respectively. Two small effects can be identified. First, the limb-darkened transits become some 0.02–0.03% deeper than those measured assuming a uniform stellar disk. But also, and very importantly in our case, the relative transit depth varies by no more than 0.01%, which is actually about 1/2 of our quoted error bars. In conclusion, the influence of limb darkening in our measurements is not significant.

4.4. Contribution of spots

HD 189733 is known to be a relatively active star (Winn et al., 2007, Pont et al. 2007a), with spots that can cause variations of $\sim 3\%$ at visible wavelengths (Strassmeier et al. 2000). These likely arise from rotational modulation over a period of 12.04 days. To set the context, the observed light variations would be equivalent to a dark spot with a radius of $1 R_{\text{Jup}}$ and effective temperature $\sim 1000\text{K}$ cooler than the photospheric effective temperature of the star. The effect of spots is

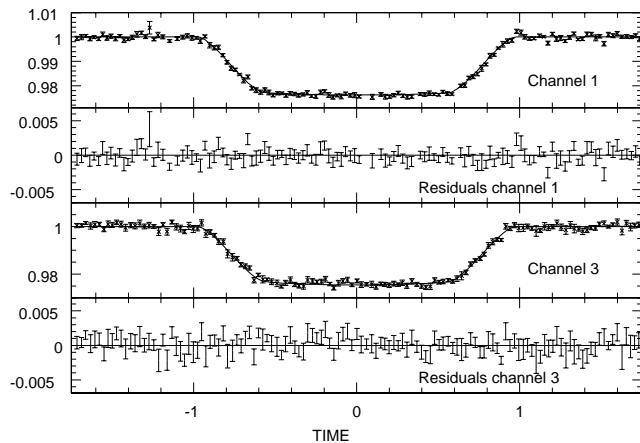


FIG. 3.— From top to bottom: the channel 1 transit curve with its Mandel and Agol (2002) model, the residuals of the fit, the channel 3 transit curve with its model, and then the residuals of the fit.

expected to be particularly important at visible wavelengths, because the contrast with the surrounding photosphere is larger.

In our case the important issue is the possible impact of spots on the determination of the planetary transit depth. Furthermore, the effect would be inexistent if spots were distributed homogeneously on the stellar surface. However, numerous surface maps of active stars, mostly obtained with the so-called Doppler tomography technique (e.g., Strassmeier 2002, and references therein), have revealed that active stars tend to have an accumulation of active areas (i.e., dark spots) at polar latitudes. A possible scenario is one in which the planet path during the transit occurs over an unspotted area of the star and therefore the resulting transit would appear deeper (since the occulted area would correspond to the brighter photosphere). Below we analyze this extreme situation and evaluate the effect on the observed differential depth of the two channels.

To address this issue we modeled the effects of spots in the bands of $3.6 \mu\text{m}$ and $5.8 \mu\text{m}$. We took the stellar parameters described in §3.1 and $T_{\text{eff}} = 3500\text{K}$, $\log g = 4.5$ for the spots. We adopted the NextGen atmosphere models (Hauschildt et al. 1999), based on the PHOENIX code. The integrated stellar flux was simulated by adding the fluxes from the photospheric and spotted regions with the appropriate weights to consider different spot areal coverages. We then calculated photometry by convolving with the IRAC passbands. Tests using this extreme model and a 20% surface spot coverage indicate that one could expect an absolute effect of about 0.19% in the measured transit depth at $3.6 \mu\text{m}$ and about 0.18% at $5.8 \mu\text{m}$. Both would be in the sense of making the spot-corrected transit shallower. As can be seen, while the correction is large in absolute terms, the difference between the two bands is of about 0.01% (in the direction of making them more different than measured), which corresponds to approximately 0.5σ of our quoted error bars. Larger spot coverages would also imply larger effects. For example, a stellar surface covered 50% with spots would result in a increased difference between the two bands by 0.05%, but this is a very extreme – and possibly unphysical – scenario.

It is interesting to evaluate the effect of spot modula-

tion when combining multi-epoch transit depth measurements. This is relevant in our case because we also consider the $8 \mu\text{m}$ measurement by Knutson et al. (2007), which was obtained with a difference of one orbital period (2.2 days). Using a spot modulation amplitude of ~ 0.03 mag it can be deduced that the spot coverage of the stellar hemisphere in view may have changed by about 2% during this time lapse. In the case of the $8 \mu\text{m}$ band the correction for such spot change in the transit depth will be around 0.01-0.02% (in either direction depending on whether the spot coverage has increased or decreased). Again, this is a small correction (less than 1σ) that corresponds to an extreme scenario. The effect is therefore negligible.

Our model also predicts that the effects in the optical wavelengths can be much larger (of the order of 0.5% or more in the observed transit depth). Therefore, the observed difference between the IR and visible radii might be due to stellar activity. Tinetti et al. (2007a) propose the presence of optically thick (in the visible) clouds/haze in the upper atmosphere as a possible explanation of this difference. Additional – and possibly simultaneous – observations in both the visible and IR are needed to draw firmer conclusions and to disentangle these two potential contributions.

4.5. Comparison with previous analysis of the same data set

In an earlier letter, Ehrenreich et al. (2007) adopted a method to analyse the IRAC data that differs from the standard ones reported in the literature and used here. In their paper, they conclude that systematic effects contaminate the final results in such a way that the error bars of Tinetti et al. (2007b) and Knutson et al. (2007) are severely underestimated. According to the authors, the accuracy in the radius determination in the IR is not of sufficient accuracy for the spectroscopic characterization of close-in atmospheres. In the remainder of this section we argue that it is not the IR data, and *Spitzer* in particular, that have insufficient quality but rather that the lack of accuracy can be attributed to shortcomings in the analysis method devised by Ehrenreich et al. As discussed below and as evidenced by the residuals in published *Spitzer* photometry (Knutson et al. 2007, Deming et al., 2007, Morales-Calderón et al., 2006), the systematic effects in the data can be estimated and robustly corrected for.

Firstly, because of a non-optimal centroid determination, Ehrenreich et al. found a larger sensitivity to pixel phase effects than the reduction presented here. Secondly, these authors expressed concern about the potential contamination by a hot pixel located 4 columns away from the central pixel of the PSF. With our adopted weighted PSF fit, this pixel was flagged and thus it is not contaminating the measurement. A third concern raised by Ehrenreich et al. was the effect of limb darkening on the measurement of the planet radius. We refer the reader back to §4.3 for detailed discussion on this point, but, in short, differential effects between the 3.6 and $5.8 \mu\text{m}$ bands are below 0.01%, i.e., 0.5 sigma. We further note that Ehrenreich et al. did not consider the contribution from star spots while this is of the same order as limb darkening effects, and especially important when comparing with the results in the visible.

Contrary to the statement of Ehrenreich et al., the 3.6 μm observations are not saturated for any part of the observation. The maximum value of the peak pixel for the 3.6 μm data is 115000 electrons which is well below the published well depth of 145000 electrons. If the observations were strongly saturated, we would expect the measured flux density to be 10% less than the predicted flux density of 1.807 Jy. Our measured flux at the beginning of the observation is 1.799 Jy which is in good agreement with expectations.

We are also at variance with the suggestions of Ehrenreich et al. about the need to observe multiple transits with the longest possible out-of-transit baseline. It has not yet been demonstrated that residual systematics would be reduced by analyzing multiple epochs. It is very likely that the pixel-phase effect will have to be treated separately for each epoch as the acquisitional pointing accuracy of *Spitzer* is ~ 1 arcsecond (a good fraction of an IRAC array pixel). The ability to coadd multiple epochs of IRAC data will tested with upcoming observations of HD 209458b as part our *Spitzer* program WET-WORLD (PI Tinetti), or, alternatively, by using multiple epochs obtained by other groups. Moreover, it is known that once the satellite settles in a repeatable jitter pattern, the timescale of systematic effects is of the order of ~ 1 hour. Thus, 2.5 hours of pre-transit observations followed by 2 hours of post transit would be our recommended observing strategy to carefully estimate and correct for systematic effects.

4.6. Comparison with previous observations

The most recent optical and IR measurements of the radius of HD 189733b are plotted in Fig. 4 with an underlying model similar to the one presented by Tinetti et al. (2007b), with the addition of hazes contributing in the visible. The b and R_* values at 3.6 and 5.8 μm are consistent with the visible values (Winn et al. 2007).

Our results are consistent, but not overlapping, with the Knutson et al. (2007) measurement at 8 μm . The three primary transit observations at 3.6, 5.8 and 8 μm with IRAC are in agreement with the predictions of Tinetti et al. (2007a) and the presence of water vapor in the atmosphere of the planet. This explanation is not necessarily in contradiction with the most recent observation of HD 189733b with the *Spitzer* Infrared Spectrograph (IRS) using the occultation – as opposed to the transit – (Grillmair et al. 2007). Fortney & Marley (2007) pointed out that this observation does not agree with the Knutson et al. (2007) secondary transit measurement at 8 μm , hence the IRS observations might have some problems in the 7.5–10 μm range. Also, the absence of atmospheric signatures in the thermal emission spectrum of HD 189733b might be explained by an isothermal atmosphere (Tinetti et al. 2007b; Fortney et al. 2006) whereas the primary transit technique allows us to probe the atmospheric content independently of the temperature gradient.

5. CONCLUSIONS

We estimated accurately the radius of the extrasolar planet HD 189733b using its primary transit, at 3.6 and 5.8 μm . The small error bars are the result of a high signal-to-noise ratio and weak influence of the limb-darkening effect in the IR. The planetary radius appears

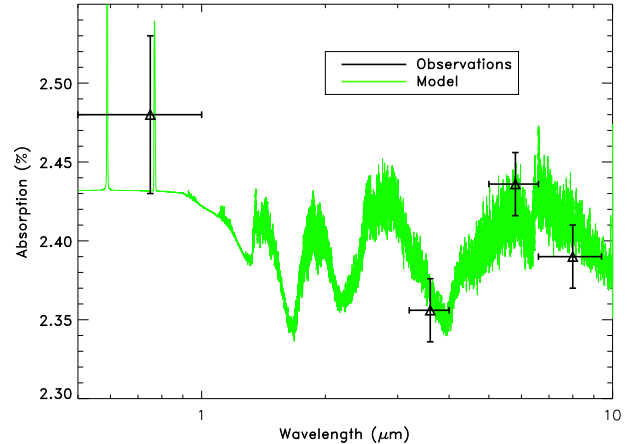


FIG. 4.— Transit depths as a function of wavelength: our two measurements at 3.6 and 5.8 μm are indicated with their error-bars. For comparison we show previous measurements at 8 μm (Knutson et al. 2007) and in the visible (Winn et al. 2007). Horizontal bars illustrate the instrument bandpasses. The solid line shows the simulated absorption spectrum of the planet between 0.5 and 10 μm . The atmospheric model includes water with a mixing ratio of $5 \cdot 10^{-4}$, Sodium and Potassium absorptions, and hazes at the millibar level in the visible. The underlying continuum is given by $\text{H}_2 - \text{H}_2$ contribution which is sensitive to the temperature of the atmosphere at pressure higher than the \sim bar level. Details of the haze free model are given in Tinetti et al., (2007b). Here, hazes are simulated with a distribution of particles peaked at 0.5 μm size. In this example haze opacity mask the atomic and molecular features at wavelength bluer than 1.2 microns. See also Brown (2001) and Pont et al., (2007b).

(1.6 ± 0.5)% larger at 5.8 μm than at 3.6 μm . The observations match the predictions by Tinetti et al. (2007a).

Detailed interpretation of these results (Tinetti et al. 2007b) combined with the 8 μm observations (Knutson et al. 2007) confirm that water vapor is the most likely explanation for the observed photometric signature in the IR. The comparison with the visible is more complex because of the possibly important role of star spots.

Our observations show that the combination of the primary transit technique and comparative band photometry at multiple wavelengths is an excellent tool to probe the atmospheric constituents of transiting extrasolar planets. Similar studies and observations should be considered for other targets, especially with the foreseen *James Webb Space Telescope*, which could observe more distant and smaller transiting planets.

We thank the staff at the *Spitzer* Science Center for their help. We are very grateful to Christophe Alard for having helped us in the data reduction phases of *Spitzer* data. His optimal centroid determination has been an important contribution to this analysis. We thank David Kipping for careful reading of the manuscript, and David Sing for providing the limb darkening coefficients. This work is based on observations made with the *Spitzer Space Telescope*, which is operated by the Jet Propulsion Laboratory, California Institute of Technology under a contract with NASA. G. Tinetti acknowledges the support of the European Space Agency. IR acknowledges support from the Spanish Ministerio de Educación y Ciencia via grant AYA2006-15623-C02-02. JPB, IR and GT acknowledge the financial support of the ANR HOLMES.

REFERENCES

- Alard, C., 2000, AAS, 144, 363
 Alard, C., 2007, A&A, in prep
 Bakos, G. Á., Knutson, H., Pont, F., et al. 2006, ApJ, 650, 1160
 Bakos, G. Á., Pál, A., Latham, D. W., Noyes, R. W., & Stefanik, R. P. 2006, ApJ, 641, L57
 Ballester, G. E., Sing, D. K., & Herbert, F. 2007, Nature, 445, 511
 Ben-Jaffel, L., 2007, ApJ, L671, L1
 Bouchy, F., Udry, S., Mayor, M., et al. 2005, A&A, 444, L15
 Brown, T. M. 2001, ApJ, 553, 1006
 Butler P., Wright J., Marcy G., et al., 2007, “<http://exoplanets.org/planets.shtml>”
 Charbonneau, D., Brown, T. M., Noyes, R. W., & Gilliland, R. L. 2002, ApJ, 568, 377
 Deming, D., Seager, S., Richardson, L. J., & Harrington, J. 2005, Nature, 434, 740
 Deming, D., Harrington, J., Seager, S., & Richardson, L. J. 2006, ApJ, 644, 560
 Deming, D., Richardson, L. J. & Harrington, J., 2007 MNRAS, in press
 Ehrenreich D., Hebrard G., Lecavelier des Etangs A., et al. 2007, ApJ668, L179
 Fazio, G. G., Hora, J. L., Allen, L. E., et al. 2004, ApJS, 154, 10
 Fortney, J. J., Cooper C.S., Showan A.P., Marley M.S. and Friedman R.S., 2006, ApJ, 652, 746
 Grillmair, C. J., Charbonneau, D., Burrows, A., et al. 2007, ApJ, 658, L115
 Hauschildt, P. H., Allard, F., Baron, E., 1999 ApJ, 512, 377
 Kurucz R. 2006, Stellar Model and Associated Spectra (<http://kurucz.harvard.edu/grids.html>)
 Mandel, K., & Algol, E. 2002, ApJ, 580, L171
 Morales-Calderón, M., Stauffer, J. R., Kirkpatrick, J. D., et al. 2006, ApJ, 653, 1454
 Pont F., et al., 2007a in press 2007arXiv0707.1940P
 Pont F., et al., 2007b MNRAS submitted
 Richardson, L. J., Harrington, J., Seager, S., & Deming, D. 2006, ApJ, 649, 1043
 Richardson, L. J., Deming, D., Horning, K., Seager, S., & Harrington, J., 2007 Nature, 445, 892
 Schneider J., 2007, <http://exoplanet.eu/index.php> “*The Extrasolar Planets Encyclopaedia*”
 Strassmeier, K. G. 2002, Astronomische Nachrichten, 323, 309
 Strassmeier, K., Washuettl, A., Granzer, T., Scheck, M., & Weber, M. 2000, A&AS, 142, 275
 Tinetti, G., Liang, M.-C., Vidal-Madjar, A., et al. 2007a, ApJ, 654, L99
 Tinetti, G., Vidal-Madjar, A., Liang, M.-C., et al. 2007b, Nature 448, 169
 Vidal-Madjar, A., Lecavelier des Etangs, A., Désert, J.-M., et al. 2003, Nature, 422, 143
 Vidal-Madjar, A., Désert, J.-M., Lecavelier des Etangs, A., et al. 2004, ApJ, 604, L69
 Winn, J. N., Holman, M. J., Henry, G. W., et al. 2006, AJ, accepted (astro-ph/0612224)